Anomalous electron transport due to multiple high frequency beam ion driven Alfvén eigenmodes

2010 Nucl. Fusion 50 084012

(http://iopscience.iop.org/0029-5515/50/8/084012)

IOP Publishing and International Atomic Energy Agency Nuclear Fusion

Nucl. Fusion **50** (2010) 084012 (11pp) doi:10.1088/0029-5515/50/8/084012

Anomalous electron transport due to multiple high frequency beam ion driven Alfvén eigenmodes

N.N. Gorelenkov[1,a], D. Stutman[2], K. Tritz[2], A. Boozer[3], L. Delgado-Aparicio[1], E. Fredrickson[1], S. Kaye[1] and R. White[1]

[1] Princeton Plasma Physics Laboratory, PO Box 451, Princeton, NJ, 08543-0451 USA
[2] Johns Hopkins University, Baltimore, Maryland 21218, USA
[3] Columbia University, New York, NY 10027, USA

E-mail: ngorelen@pppl.gov

Received 15 November 2009, accepted for publication 28 June 2010
Published 28 July 2010
Online at stacks.iop.org/NF/50/084012

Abstract

We report on the simulations of recently observed correlations of the core electron transport with the sub-thermal ion cyclotron frequency instabilities in low aspect ratio plasmas of the National Spherical Torus Experiment. In order to model the electron transport the guiding centre code ORBIT is employed. A spectrum of test functions of multiple core localized global shear Alfvén eigenmode (GAE) instabilities based on a previously developed theory and experimental observations is used to examine the electron transport properties. The simulations exhibit thermal electron transport induced by electron drift orbit stochasticity in the presence of multiple core localized GAE.

(Some figures in this article are in colour only in the electronic version)

1. Introduction

Anomalous electron heat transport was observed in National Spherical Torus Experiment (NSTX) recently when strong, up to $P_{\rm NBI} = 6$ MW, NBI heating was applied in both H- and L-mode discharges [1]. Subsequent analysis allowed to infer high rates of the electron heat conductivity $\chi_{\rm e} \geqslant 10\,{\rm m}^2\,{\rm s}^{-1}$. At the same time strong high frequency MHD activity, $f = 0.5$–1 MHz, increasing with the applied NBI power, was measured at the plasma edge and in the plasma core. The high frequency spectrum contains multiple instabilities, which can be interpreted as the instabilities of the global Alfvén eigenmodes (GAEs) localized in the core of the plasma and excited by the beam ions [2].

The anomalous electron transport potentially can have significant implications for future fusion devices, especially low aspect ratio tokamaks. It can severely limit the range of plasma operation performance.

NSTX is a low aspect ratio fusion experiment [3], which presents a great opportunity for studying energetic ion physics due to strong super Alfvénic population of beam injected fast ions having central beta in the range, $\beta_{\rm f} = 5$–20%, in the plasma with a characteristic central beta, $\beta_{\rm pl} = 10$–40%, and a ratio of the birth velocity to the Alfvén velocity in the range $v_{\rm b}/v_{\rm A} = 2$–4.

[a] Author to whom any correspondence should be addressed.

Two mechanisms responsible for the anomalous electron transport due to high frequency activity in NSTX are of interest. The first is the resonance interaction with bulk (1–2 keV energy) electrons. The second is the stochastization of the electron drift motion in the presence of multiple instabilities, which was proposed recently [4]. It is based on the beam ion excitation of multiple core localized GAE instabilities, which at sufficiently strong amplitudes result in stochastic electron drift orbits that in turn can cause the anomalous electron transport. In this paper we investigate this hypothesis in detail using the set of test functions employing numerical simulations with the help of the guiding centre code ORBIT [5], which follows thermal electron trajectories. The second mechanism turns out to be the dominant one for the electron transport in our simulations when multiple modes are present. This is different from previously suggested low frequency GAE-induced electron heat conductivity, which required coherent, resonant electron–GAE interactions and the introduction of the parallel electric field due to the coupling of GAEs and kinetic Alfvén waves (KAWs) [6]. Further development of the resonant mechanism and the following alternative explanation of the anomalous electron transport in NSTX has been offered more recently [7]. Our simulations imply that both passing and trapped electrons have broad response to the perturbations in the phase space (namely in pitch angle, $\lambda = (1 - v_\parallel^2/v^2)B_0/B$, and energy, $\mathcal{E}$, where $v_\parallel$ is parallel to the equilibrium magnetic field vector, $\boldsymbol{B}_0$, velocity component).

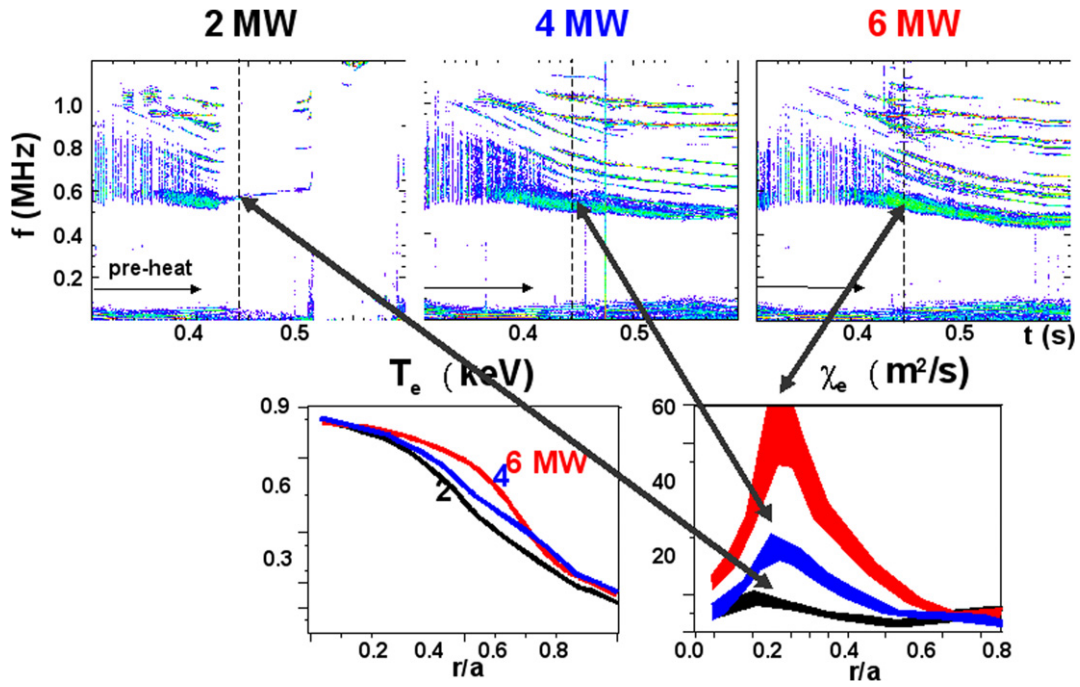

Figure 1. Correlation of the high frequency MHD activity with the flattening of thermal electron temperature profiles near the plasma centre as reproduced from [1] for NSTX shot #120438.

It is interesting that the characteristic frequencies of transit and bounce motion of electrons are close to the mode frequencies observed in the range 0.5–1 MHz and perhaps can contribute to the diffusion via the beat-wave resonances. Characteristic thermal passing electron transit frequency in NSTX plasmas is $f_{te} = (1/2\pi)(v_{\|}/qR) = 1.5$ MHz evaluated for electron temperature $T_e = 1$ keV, safety factor $q = 2$ and major radius $R = 1$ m, whereas trapped electron bounce frequency $f_{be} = (1/2\pi)(v_{\perp}/qR)\sqrt{r/2R} = 400$ kHz at $q = 2$, $r/a = 0.2$, where r is the minor radius of a magnetic surface and a is the plasma minor radius. In experiments q can change so that this estimate should be adjusted. Because of such close frequency relations the adiabatic contribution to the fluctuations of particle trajectories in response to the perturbations remains significant and if coupled with the stochastization mechanism can induce particle diffusion.

Application of the guiding centre code, ORBIT, shows that the required level of the electron heat conductivity, $\chi_e \geqslant 10\,m^2\,s^{-1}$ is established in simulations with $>\sim 20$ intermittently unstable GAEs with the internal density perturbation amplitudes on the order of $\delta n_e/n_e = 10^{-3}$. This is close to the experimentally measured plasma density fluctuations inferred from the density averaged over the sight line of the high-k diagnostics operated in the interferometric mode. Our simulations address the requirements for GAE structure, amplitudes and the number of modes to achieve the electron heat diffusivity resulting from experimental analysis. Results from the comparisons of the theory and recent NSTX experiments are presented. In this paper we focus not on exact comparison with the experiments, but on the theoretical and numerical insights of the electron transport mechanism due to multiple GAE instabilities with the test functions of GAE structures. Such insight is needed for further experimental and theoretical studies. In addition, to account for the effects due to the collisions we will use electron Coulomb scattering frequency $\nu_e/\omega_{ce} = 3 \times 10^{-7}$ ($\omega_{ce} = 0.7 \times 10^{11}\,s^{-1}$), and assume that e–i collisions double its value.

This paper is organized as follows. In section 2 we outline key experimental evidence of the anomalous electron transport in NSTX plasma. Then we present the numerical model in section 3. Results of the simulations and their interpretations are given in section 4. It turns out that the effect of the parallel electric field is important for the electron diffusion even when it is small. The relevant simulation results are given in section 5. The main results of the work are summarized in section 7.

2. Experimental evidence of anomalous electron transport

Experimental results from NSTX were reported earlier [1] and showed that at high NBI power, electron temperature does not increase in the centre during the heating phase even when the applied power increases from $P_{NBI} = 2$, to 4 and then to 6 MW. Instead, the T_e profile becomes flat in both L- and H-mode discharges near the plasma centre, $r/a \leqslant 0.4$, as can be seen in figure 1. Here we studied NSTX plasma with parameters that are typical for NSTX operations: aspect ratio, $R_0/a = 0.85\,m/0.61\,m = 1.4$, NBI energy of 70–90 keV, plasma current $I_p = 0.8$–1 MA, equilibrium magnetic field $B_{T0} = 0.45$–0.55 T and flat density profile with a central density value (5–6) $\times 10^{13}\,cm^{-3}$. The safety factor was close to, but above 1, so that the sawtooth oscillations are avoided.

An analysis of the overall plasma performance using the TRANSP code was conducted to infer the thermal electron heat conductivity. The code solves the power balance equations and accounts for the heat diffusion via various channels. It uses several constraints from the measurements of the internal plasma parameters, such as electron and ion temperature and

density profiles as well as the neutron flux. Such analysis required strong χ_e so that at $P_{NBI} \geqslant 4$ MW TRANSP predicts characteristic $\chi_e \geqslant 10\,m^2\,s^{-1}$. The predictions for the low end of the χ_e range seem to be robust even with the uncertainties in the measurements and in the analysis. The robustness in part comes from the dominant heating channel of electrons by the beams. Only below critical energy, $\mathcal{E}_{bcrit} \simeq 20T_e \simeq 20$ keV, beam ions transfer their energy to the thermal ions, so that the majority of the NBI power is absorbed by electrons. Beam ions are expected to have peaked profiles with insignificant low frequency MHD such as in the studied plasmas. This is supported by the neutral particle analyzer (NPA) measurements. Further, in many experiments the localization region of low frequency Alfvénic activity is at the minimum of the safety factor surface, which is outside the plasma centre. Thus, the low frequency modes are decoupled from the mechanism of the electron transport. As detailed analysis shows, the flattening of the fast ion profiles is not consistent with the neutron flux and NPA measurements [8].

Thermal ion transport stays low, within the neoclassical range, an order of magnitude lower than χ_e, in high NBI power shots. This suggests that the stochastic thermal ion heating mechanism [9] is not applicable in these plasmas. We also note that central T_e flattening is accompanied by a temperature increase at the periphery, which is reflected in χ_e radial dependence and in the fact that total heating power substantially increases.

An independent support of TRANSP inferred χ_e value comes from a special experimental study of the induced T_e perturbation propagation in high NBI power discharges [8]. In those experiments applied Li pellet ablates in a shallow region near the plasma edge and introduces T_e perturbation propagating rapidly in the high beam power plasmas towards the plasma centre. Such a technique was applied to edge-localized modes (ELMs) studies and ELM effects on electron transport [10]. The rate at which the temperature perturbation propagates allows observation of radial dependence of the χ_e value independently of TRANSP results. From those perturbative experiments χ_e emerges in the range of tens $m^2\,s^{-1}$, which is in the same ballpark as the predictions from TRANSP. The absolute value of temperature perturbation is relatively small and amounts to $\sim 10\% T_e(0)$ and can be comparable to the edge electron temperature. As an example we show contours of the electron temperature in figure 2 measured by the SXR diagnostic in the (time, T_e) plane. T_e perturbation is shown to propagate from the edge ($t \simeq 453$ ms) to the plasma centre ($t \simeq 455$ ms). The total time of the cold front propagation is very short, on the order of 2 ms.

The time dependence of the perturbation propagation can be obtained from the diffusion equation. If the perturbation gradient is strong, $T_e/\nabla T_e < r$, and the perturbation is Gaussian in radius the radial coordinate of the perturbation front should evolve according to

$$r_{pert} = a - \sqrt{t\,\chi_e(r)}.$$

Thus, in observations we should look for the fastest change in $T_e(t)$ (point of strongest slope gradient of the $T_e(t)$ dependence in figure 2) to characterize the front propagation. The corresponding curve of the T_e perturbation front is shown in figure 2 as a thick dashed line. This curve is different from the curve used in [8], where the minimum of the perturbation in time was used as a reference point to characterize the perturbation propagation. Figure 2 corresponds to when the beam power was changed from 4 MW in the pre-heat phase to 6 MW. Inferred χ_e reached $100\,m^2\,s^{-1}$, which is consistent with the TRANSP simulation (see figure 1). A more accurate comparison requires more detailed study of the SXR diagnostic modelling. If the power is changed to 2 MW the perturbation does not propagate beyond $r/a \simeq 0.5$ to the plasma centre. This points to low χ_e value.

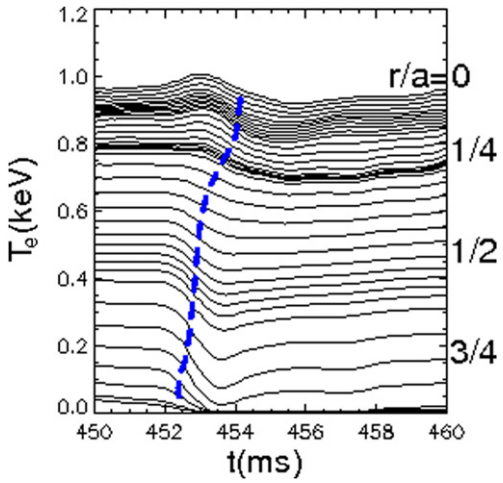

Figure 2. The SXR diagnostic measured the electron temperature evolution during the shallow pellet perturbation in NSTX shot #120440 with 6 MW beam power. NBI power is increased from 4 MW in the pre-heat phase.

We also note that the behaviour of the T_e perturbation front propagation indicates the diffusive process rather than the presence of the convective cells, except near the very centre of the plasma, $r/a < 0.25$.

Subsequent analysis of the plasma with regard to the microscopic stability performed using the linear GS2 code indicated that the central gradient is too weak to sustain any known drift instability at the growth rate above the observed shearing rate of the plasma rotation [8]. Measurements of the wavevector spectrum with high-k diagnostic did not show any evidence of the ETG driven instability at frequencies where they are usually seen.

On the other hand, a correlation between the flattening of the electron temperature and the high frequency activity was observed as shown in figure 1. The frequency range where instabilities are seen, 0.5–1 MHz, is typical for NSTX plasma. This frequency range was shown to be populated by both GAEs [2] and compressional Alfvén eigenmodes (CAEs) [11]. The mode identification was based on the observed instability frequency evolution and its polarization. The caveat in the polarization measurements is that recent simulations using HYM code [12] have demonstrated that the GAEs having shear Alfvén polarization, $\delta B_\perp > \delta B_\parallel$, in the plasma centre can have different polarizations at the plasma edge, $\delta B_\perp < \delta B_\parallel$, which is the property of CAEs. Thus, to robustly identify the instability one has to measure its internal structure in addition to the polarization and frequency spectrum. GAEs are localized primarily near the plasma axis [2], whereas CAEs are

localized closer to the plasma edge [13], but can be also present near the plasma centre [14]. One important theoretical result is that GAEs with different m, n pairs have different frequency evolutions as follows from a simple GAE dispersion relation: $\omega \simeq v_A(m - nq)/qR_0$. Based on the frequency evolution of the peaks in the spectrum in figure 1 we can conclude that some of the peaks evolve independently in time. This means that GAEs are apparently excited by the beams. More detailed structure measurements and mode identification are required for more accurate comparisons with the experiment.

3. Model for numerical study of GAE driven electron transport

3.1. GAE perturbation

We use previous results of theoretical findings and numerical modelling to set up the GAE test functions for e-transport investigations.

First, we note that conventional GAEs are localized just below the minimum in the Alfvén continuum [15]. GAEs were studied for the case when the continuum has a minimum between the plasma centre and the edge. Typically with flat n_e profiles near the plasma centre in NSTX and monotonic q profiles, Alfvén continuum has a minimum at $r = 0$. This case was also shown to have core localized GAEs in both theory and numerical simulations [2, 16]. It follows that to predict GAE localization and the width one has to know q profile with very good accuracy, which is often difficult to achieve in experiments. Instead, in the following numerical studies we set up all GAEs to be localized at $r_0/a = 0.2$ (where TRANSP predicts the peak of χ_e), having one poloidal harmonic, m, and Gaussian radial structure at radial width proportional to m^{-1}, which directly follows from the theory [2]. Many radial solutions can exist at each m, n pair, but we will use only the lowest one, which corresponds to the widest GAE radial structure and are likely to be more unstable than the higher radial number solutions.

At the high frequencies of interest we can neglect the compressibility of GAEs and leave only flute-like perturbation, which implies the following form for the perturbed magnetic field [5]

$$\delta \boldsymbol{B} = R_0 \nabla \times (\alpha \boldsymbol{B}_0), \tag{1}$$

where B_0 is the equilibrium magnetic field, and the sum over various modes is assumed:

$$\alpha = \sum_{j=1}^{N} \alpha_j = \alpha_0 \sum_{j=1}^{N} \mathrm{e}^{-\mathrm{i}\omega_j t + \mathrm{i}m_j\theta - \mathrm{i}n_j\varphi} \cdot \mathrm{e}^{-m_j^2(r-r_0)^2/\delta r^2} + \text{c.c.} \tag{2}$$

Here ω_j, m_j and n_j are the frequency, poloidal and toroidal mode numbers of the jth mode. All the GAEs are assumed to have the same amplitude α_0. We also fix n to be negative ranging from -1 to -7 (counter to the plasma current propagation), which follows from the magnetic coil measurements of GAE spectrum in the frequency range of interest. For each n we vary the poloidal mode number and check the simplified GAE dispersion relation

$$\omega_j = v_A k_{\|j} \simeq v_A \frac{m_j - n_j q}{q R_0} \tag{3}$$

to verify if the mode frequency falls into the frequency range 0.5 to 1 MHz of MHD activity. With the plasma parameters of the analysed NSTX shot up to $N = 31$, modes can exist in this frequency range with the rotation effect included. We do not study the stability criteria for each mode, so that some of the modes used in the simulations could be stable. It turns out that for the stochastic diffusion due to GAEs it is sufficient to include only some of $N = 31$ GAEs. It will be shown in section 4.3 that the stochastic threshold is achieved in this case at $N >\sim 16$, which is also sensitive to the mode amplitude.

Given the perturbations, equation (1), the radial component of GAE perturbed magnetic field can be approximated as

$$\delta B_r/B_0 \simeq \mathrm{i}k_\theta \alpha R_0 = \mathrm{i}\alpha m R_0/r. \tag{4}$$

For the baseline case of the simulations we consider, $q_{\min} \simeq 1.3$, $\alpha_0/R = 4 \times 10^{-4}$, its characteristic value is $\delta B_r/B_0 \simeq 0.5 \times 10^{-2}$ and $\delta r = 0.4a$.

Perturbation in the form of equation (1) allows for the finite parallel electric field, which is not compatible with the ideal MHD model widely used in GAE theory. Because of its strong effect on electron dynamics one has to be sure that $E_\|$ is zero in the cold plasma limit, i.e. the electrostatic polarization potential needs to be introduced via the equation

$$E_\| = -\nabla_\| \phi - \frac{1}{c}\frac{\partial \alpha B_0 R_0}{\partial t} = 0 \tag{5}$$

for each eigenmode, which implies that for one mode denoted with the subscript j the linear approximation for the electrostatic potential is

$$\phi_j = \omega_j \alpha_j B R_0/c k_{\|j}. \tag{6}$$

Nevertheless, even the ideal MHD GAE structure allows for a small but finite parallel electric field. Its value can be found using the quasi-neutrality condition including such effects as thermal ion finite Larmor radius (FLR), electron drift frequencies, two fluid effects and fast ions. One can show that all those effects are of the same order as the FLR effect if computed perturbatively given the ideal MHD GAE structure. For the FLR effect we can define parallel electric field potential $E_\| = -\nabla\Psi$ (see, for example, [17])

$$\Psi_j = \phi_j \frac{b_i}{b_i + 1}, \tag{7}$$

where $b_i = (k_\perp \rho_i)^2/2$ and $k_\perp \simeq k_\theta$. It is consistent with vanishing $E_\|$ in the zero FLR limit corresponding to the ideal MHD. In the NSTX baseline case we estimate $b_i \simeq 0.5 \times 10^{-4}$ given the ideal MHD GAE structure. At that level $E_\|$ has a small effect on the electron transport. Another source of the finite parallel electric field implicitly present in simulations comes from the second order corrections to equation (5), which is also small as seen in simulations. The discussion of its contributions to ϕ is given in appendix A.

3.2. Use of particle code for heat diffusion simulations

One can show that thermal ions do not interact with the high sub-cyclotron frequency oscillations of interest due to their

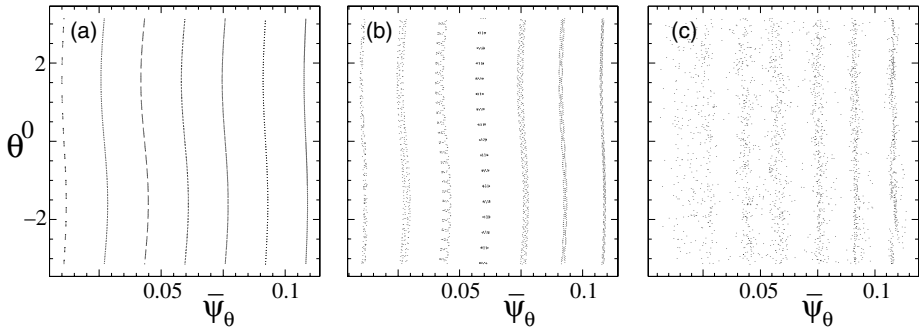

Figure 3. The electron Poincaré plot in the plane $\{\bar{\psi}, \theta^0 = \omega_1 t + n\varphi\}$ with $\bar{\psi}$ being the poloidal flux normalized to its edge value. The baseline case is considered with $\alpha_0/R = 4 \times 10^{-4}$ and $\delta E_\parallel = 0$.

low velocities. Fast ions, as we argued, provide the drive for GAE instabilities, but their density is negligible in comparison with the background density. Thus one can expect that the net thermal electron particle transport is negligible. This requires the introduction of the ambipolar electrostatic potential to compensate for the radial electron particle flux. If the electron distribution function is

$$F_e = n_e \exp[-(\mathcal{E} + e\phi)/T_e](m_e/2\pi T_e)^{3/2}, \tag{8}$$

the electrostatic ambipolar potential can be found via

$$\Gamma_e = \int D_e F_e \left(-\frac{e\phi'}{T_e} + \frac{n_e'}{n_e} + \frac{\mathcal{E}T_e'}{T_e^2} - \frac{3}{2}\frac{T_e'}{T_e}\right) \mathrm{d}^3 v = 0, \tag{9}$$

where prime means radial derivative. It follows from equation (9) that the ambipolar potential is zero as expected for the Maxwellian distribution with a flat density profile. For the arbitrary distribution function such as found in numerical simulations we find

$$\frac{e\phi'}{T_e'} = \left\langle D_e \left[\frac{(\ln n_e)'}{(\ln T_e)'} + \frac{\mathcal{E}}{T_e} - \frac{3}{2}\right]\right\rangle \Big/ \langle D_e \rangle,$$

where $\langle f \rangle = \int F_e f \, \mathrm{d}^3 v / \int F_e \, \mathrm{d}^3 v$. We also find for the distribution close to Maxwellian

$$q = \int \mathcal{E} D_e F_e \left[-\frac{e\phi'}{T_e} + \frac{n_e'}{n_e} + \frac{\mathcal{E}T_e'}{T_e^2} - \frac{3}{2}\frac{T_e'}{T_e}\right] \mathrm{d}^3 v$$

$$= n_e \frac{3}{2} D_e T_e' = n_e \chi_e T_e'. \tag{10}$$

Whereas for the numerical distribution

$$\frac{\chi_e}{D_e} = \frac{\left\langle \mathcal{E} D_{ev} \left[-\frac{e\phi'}{T_e'} + \frac{(\ln n_e)'}{(\ln T_e)'} + \frac{\mathcal{E}}{T_e} - \frac{3}{2}\right]\right\rangle}{T_e \langle D_{ev} \rangle}$$

$$= \frac{\langle \mathcal{E}^2 D_{ev} \rangle}{T_e^2 \langle D_{ev} \rangle} - \frac{\langle \mathcal{E} D_{ev} \rangle^2}{T_e^2 \langle D_{ev} \rangle^2}. \tag{11}$$

This expression is important as it allows to infer χ_e from the particle diffusivity, which is easily computed using particle codes, such as ORBIT.

4. ORBIT modelling

4.1. Single electron motion

Guiding centre code ORBIT [5] is employed here with the perturbation in the form equation (1). The underlying processes responsible for the stochastic electron transport can be understood from single electron dynamics.

First, we study the single electron motion in the presence of GAEs for the baseline case. It is possible to construct the Poincaré map in the plane $\{\bar{\psi}, \theta^0 = \omega t + n\varphi\}$ for one mode. Trapped particles with only one mode included, $(m, n) = (3, -1)$ at $f = 510$ kHz, form a map shown in figure 3(*a*). When the second mode is added we show the Poincaré map in the plane with the phase determined by the characteristics of the first mode, $\theta^0 = \omega_1 t + n\varphi$. In both cases one can see the secular motion of electrons, which is bounded in the radial direction. However, when multiple modes are included, such as the $N = 20$ case shown in figure 3(*c*), the electron motion becomes stochastic.

Perturbed electron motion in the direction perpendicular to the equilibrium magnetic field can be described by two effects, the magnetic field bending and the drift due to the perpendicular electric field:

$$\delta \boldsymbol{v}_\perp = v_\parallel \frac{\delta \boldsymbol{B}_\perp}{B_0} + \frac{c}{B_0^2}[\delta \boldsymbol{E} \times \boldsymbol{B}_0], \tag{12}$$

where δ refers to the perturbed quantities. Radial displacement of an electron, ξ_r, can be found from here using equations (4) and (5):

$$\frac{\mathrm{d}\xi_r}{\mathrm{d}t} = \frac{\mathrm{d}\delta B_r}{\mathrm{d}t}\frac{1}{\mathrm{i}k_\parallel B_0} + \frac{ck_\theta \delta E_\parallel}{k_\parallel B_0} - \frac{(\boldsymbol{v}_{dr}\nabla)\delta B_r}{\mathrm{i}k_\parallel B_0} = \frac{\mathrm{d}\delta B_r}{\mathrm{d}t}\frac{1}{\mathrm{i}k_\parallel B_0}$$

$$+ \frac{ck_\theta \delta E_\parallel}{k_\parallel B_0} + \frac{(\boldsymbol{v}_{dr}\delta \boldsymbol{E})ck_\theta}{v_A k_\parallel B_0}, \tag{13}$$

where $\boldsymbol{v}_{dr}$ is the toroidal drift velocity of electrons. The full derivative, first term in the rhs of this equation, is integrable and corresponds to the adiabatic electron motion. Thus, without the perturbed electric fields there is no net radial diffusion. The second and third terms on the rhs are non-adiabatic, which can result in the radial diffusion in the case of a few modes. We note that parallel electric field and the toroidal drift affect both non-resonant and resonant electrons. $E_\parallel$ was used to describe the resonant electron interaction in [6]. As we will show the resonant coherent motion of electrons is destroyed in the presence of multiple modes and is less relevant to our problem. This conclusion is the result of the numerical study illustrated in figure 5. If the second and the third terms of equation (13) are small we find the characteristic electron radial displacement:

$$\xi_r = \frac{\delta B_r}{\mathrm{i}k_\parallel B} = \alpha R_0 \frac{k_\theta}{k_\parallel}. \tag{14}$$

It also follows that the equation for ξ_r can be rewritten in the form

$$\frac{\mathrm{d}\xi_r}{\mathrm{d}t} \simeq -\mathrm{i}(k_\theta R_0) v_\parallel \alpha \left(1 - b_\mathrm{i}\sqrt{\frac{m_\mathrm{e}}{\beta_\mathrm{e} m_\mathrm{i}}} - \frac{k}{k_\theta k_\parallel R}\sqrt{b_\mathrm{i}}\sqrt{\frac{2m_\mathrm{e}}{m_\mathrm{i}}}\right). \tag{15}$$

Two last terms in the rhs of equations (13) and (15) are related as $\sqrt{b_\mathrm{i}} : \sqrt{2\beta_\mathrm{e}}/k_\parallel R$, which means that with the NSTX parameters of interest and with the ideal MHD GAE structures, the parallel electric field term is smaller and the non-adiabatic interaction is mediated by the perpendicular electric field and the toroidal drift. The last term in equation (13) was neglected in [6]), which was justified in that work by an assumed significant increase in b_i from the ideal limit.

Thus, the mechanism of electron diffusion follows. The first term in equation (13) determines the radial electron displacement, whereas the third term (toroidal drift across the field line) makes the electron motion non-integrable by dephasing it from the secular adiabatic motion (detaching from the field line). The electron–GAE dephasing introduces electron orbit stochasticity when many GAEs are present.

We estimate the characteristic dephasing time, τ_deph, from the requirement that the third term in the rhs of equation (13) introduces radial displacement sufficient to change electron phase by $\Delta r k_r \simeq \pi$. From equations (13) and (6) we find that the inverse dephasing time is proportional to the toroidal drift velocity and the mode amplitude:

$$\tau_\mathrm{deph}^{-1} = \frac{k_r k_\theta R_0}{\pi k_\parallel} \boldsymbol{v}_\mathbf{dr} \boldsymbol{k} \alpha. \tag{16}$$

It is important to note here that in both equations (14) and (16) α includes all the modes. The resulting sum of the modes depends strongly on the particular spectrum used in simulations. It can be shown that in our case the sum of GAEs, $\sum_j \alpha_j$, along the particle orbit is limited by the maximum value, which increases with N. It is trivial in the case of two modes, but gets more complicated in the case of multiple modes, which is difficult to compute analytically. Leaving the details to future work we offer an empirical expression for the limit value of the α variation, $|\alpha| \leqslant \alpha_0 N N_\mathrm{thr}/\sqrt{N^2 + N_\mathrm{thr}^2}$, which appears to be valid for low to medium N, where $N_\mathrm{th} \simeq 15$. We also note that at high N, $|\alpha| < \alpha_0 N_\mathrm{thr}$.

4.2. Particle diffusion

In the numerical study we load electrons with the Maxwell isotropic distribution function on a certain flux surface and monitor how their radial positions evolve in the presence of multiple GAEs and collisions. Electrons are allowed to drift in the equilibrium magnetic field over a long time period compared with their transit, precession periods around the torus and the oscillation periods of GAEs. If the process is diffusive then we should observe linear in time behaviour of the average over particles of the flux variable, $\langle \Delta\psi^2 \rangle(t)$, where $\Delta\psi = \bar{\psi} - \bar{\psi}_0$ and $\bar{\psi}_0$ is the particle initial normalized poloidal flux.

In the example shown in figure 4 we used the baseline case with $\alpha_0 = 4 \times 10^{-4}$, $\bar{\psi} = 0.06$, $\bar{\psi}_0 = 0.04$, $T_\mathrm{e} = 1\,\mathrm{keV}$ and $N = 31$. One can see almost linear dependence

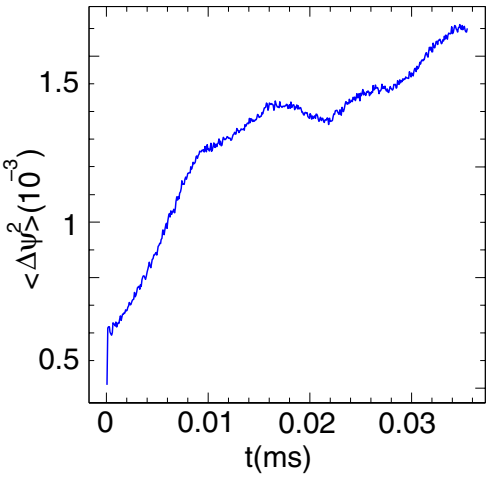

Figure 4. Time evolution of the poloidal flux $\langle \Delta\psi^2 \rangle(t)$ averaged over the electron distribution in the presence of multiple GAEs.

of $\langle \Delta\psi^2 \rangle$ in time from $t =\sim 0$ (after electrons prompt relaxation) to $t = 0.012\,\mathrm{ms}$. It is well known that the linear dependence is characteristic for the particle diffusion with the initial distribution close to the delta function in radius. By $t = 0.012\,\mathrm{ms}$ most effected electrons reach the boundaries of the GAE localization region and the effects of the mode finite width become important.

It is interesting to look into the phase space picture of the electron diffusion. In figure 5 we plot the contour map of the electron displacement in the plane-pitch angle, $\lambda = \mu B_0/\mathcal{E}$, energy, $\mathcal{E}$(keV), where μ is the adiabatic moment. Shown is the deviation of the particle poloidal magnetic flux from the mean poloidal magnetic flux over the particle distribution:

$$\langle |\psi^2 - \langle \psi \rangle^2| \rangle_{\mathrm{d}v},$$

where $\mathrm{d}v$ means that the average is taken over the vicinity (small rectangle on the contour map) of a point in the map plane. In figure 5(*a*) the deviation is plotted for the intermediate values of the GAE amplitudes, $\alpha_0 = 10^{-4}$ and $\nu_e = 0$, whereas for figure 5(*b*) we used much larger amplitudes $\alpha_0 = 4 \times 10^{-4}$. In both cases we had $N = 31$ modes and $\bar{\psi} = 0.05$. For weak GAE amplitudes two regions are seen to have stronger, perhaps resonant, interactions with the modes. First is the passing particle region, approximately at $\lambda = 0.3$, $E = 3\,\mathrm{keV}$, at which energies electrons do not have direct transit resonance, but may have some beat frequency transient resonances with the frequencies $\Delta\omega_{jk} = \omega_j \pm \omega_k$. The second region is the trapped electron region, near $\lambda \simeq 1$ in a broad energy range. Simulations indicate that it is broad due to many frequencies present and thus many trapped electrons potentially may be in resonant interaction.

GAEs with strong amplitudes smear the regions of strong coherent electron–GAE interactions, such as at $\alpha_0 = 4 \times 10^{-4}$ shown in figure 5(*b*). Clearly the interaction with electrons is much broader in the phase space at high mode amplitude, which indicates that the resonant structures are not established. Application of the expression, equation (11), to case (a), $\alpha_0 = 10^{-4}$, gives very low electron heat conductivity $\chi_\mathrm{e} < 1\,\mathrm{m^2\,s^{-1}}$, whereas at $\alpha_0 = 4 \times 10^{-4}$ we find $\chi_\mathrm{e} \simeq 10\,\mathrm{m^2\,s^{-1}}$, which is marginally close to the TRANSP inferred values.

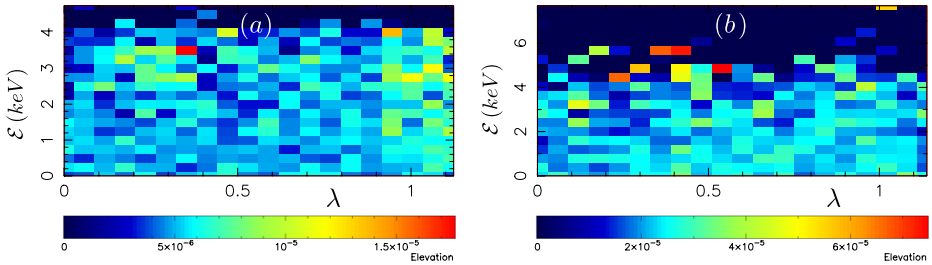

Figure 5. Contour map of electron displacement in the phase space. Mean values $\langle|\psi^2 - \langle\psi\rangle^2|\rangle_{dv}$ are plotted in each bean, where the outer averaging is taken in the vicinity of each point of the plane. Elevation is in arbitrary units reflected in the linear colour scheme. (*a*) is for low GAE amplitudes $\alpha_0 = 10^{-4}$, whereas (*b*) is for high amplitude $\alpha_0 = 4 \times 10^{-4}$.

As we argued in the discussion after equation (13) the decorrelation of the electron GAE interaction is due to the oscillating electric fields. For the coherent wave particle interaction, which is expected in the case of resonant interaction, the particle energy change is proportional to the change in the particle radial position $\Delta\psi \sim \Delta\mathcal{E}$ [18]. If the resonances are important and if they remain coherent over the simulation time they should be recognizable as structures in the electron test particle simulations because only a finite number of low n modes is present and because the frequencies of all the modes are close to each other. We illustrate such dependence obtained in simulations in figure 6, where no sign of resonant structures can be identified. This lends support to our interpretation of the mechanism of electron diffusion to be broad in the phase space in which the coherent interaction with the GAEs is not established and electron drift trajectories are stochastic.

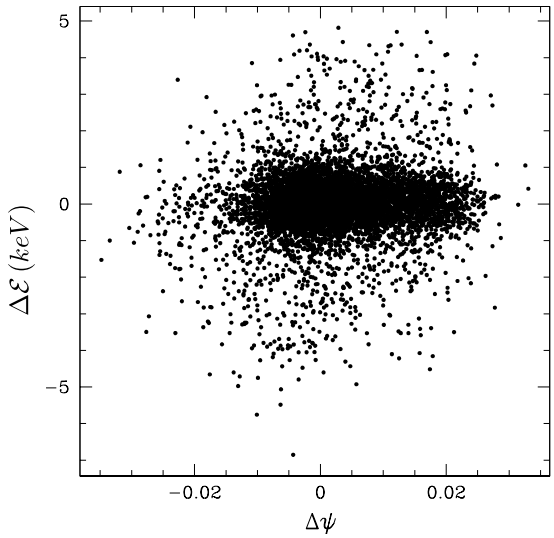

Figure 6. The change in the electron radial position shown via the change in the normalized poloidal flux versus the change of its energy for the baseline case. Particle parameters are taken at the end of the run shown in figure 4.

4.3. Thermal electron heat conductivity dependences

Because of the importance of the stochastic threshold onset we show the dependence of the heat electron conductivity on the number of GAEs included in the simulations in figure 7. In this study we increased the number of modes by varying n from -1 down and varying m's to fit the 0.5 to 1 MHz frequency range.

At small N's χ_e is small and only weakly depends on N. This is consistent with our argument about the adiabaticity of the electron motion. Note that the role of resonances is weak at these amplitudes as only a narrow region of the phase space is affected. Electron diffusivity jumps by almost two orders of magnitude at $N > 16$. The modes included in simulations are all close in values of $k_\parallel$ and frequencies, and interchanging them produces similar results. At $N >\sim 16$ we find a plateau: weak dependence on the number of modes, which is a surprising result.

In simulations we observed various dependences with regard to the GAE amplitudes. The results of such study are shown in figure 8.

These results together with the single particle characteristic motion (see section 4.1) help to construct the expression for χ_e and to understand its dependences on some plasma and GAE parameters. The radial particle displacement is randomized by the toroidal drift dephasing with the characteristic time given in equation (16). Thus we can construct the following expression having in mind

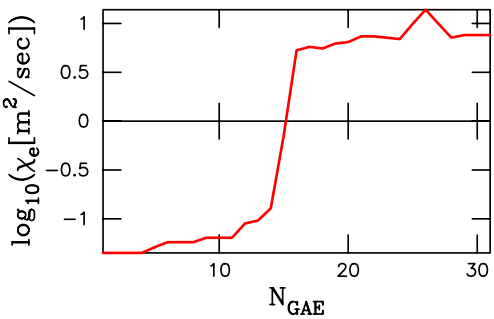

Figure 7. Electron heat conductivity dependence versus the number of applied GAEs. The results are obtained for the baseline case $\nu_e/\omega_{ce} = 6 \times 10^{-7}$, $\bar{\psi} = 0.06$, $\alpha_0/R = 4 \times 10^{-4}$.

equation (14) and characteristic values $k_\parallel \simeq 2m/qR$, $m = 3$, $\alpha_0 = 4 \times 10^{-4}$ $q = 1.3$, $N = 20$:

$$\chi_e = \frac{3}{2}\xi_r^2 \tau_{deph}^{-1} = \alpha^3 R_0^3 \frac{3k_\theta^3}{2k_\parallel^3} \frac{k_r k_\perp v_{dr}}{\pi}, \qquad (17)$$

which is evaluated to $\chi_e \simeq 4\,m^2\,s^{-1}$. This is reasonably close to the observed values of the thermal heat conductivity at the plateau given the spread of used GAE parameters.

The expression for the diffusion coefficient we found has cubic dependence on the mode amplitude $\chi_e \sim \alpha^3$. This is

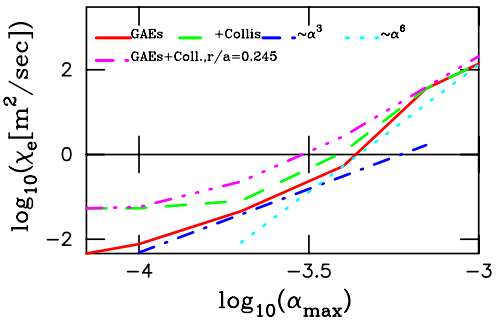

Figure 8. Electron heat conductivity versus GAE amplitude dependences. Solid curve corresponds to the χ_e without collisions at $\bar{\psi} = 0.05$, dashed curve includes collisions, dash–dot–dot–dot curve includes collisions but is obtained at $\bar{\psi} = 0.06$. For comparison, two lines, dash–dot and dot–dot, are plotted with α^3 and α^6 dependences.

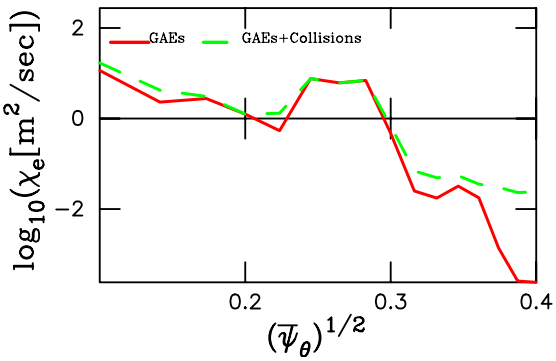

Figure 9. Radial dependence of thermal electron conductivity obtained for the baseline case at $\alpha_0 = 4 \times 10^{-4}$ with (dashed line) and without (solid line) collisions.

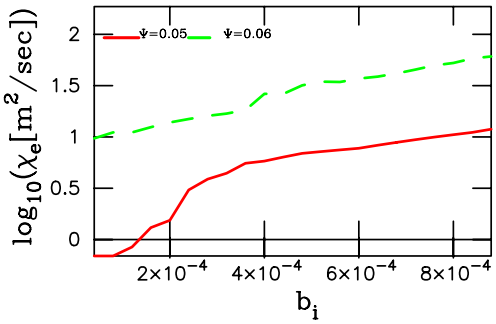

Figure 10. Parallel electric field dependence of the electron heat conductivity for the baseline case $\nu_e = 0$, $\alpha_0 = 4 \times 10^{-4}$. Two curves correspond to two different initial radial positions of electrons as indicated.

different from the diffusion due to the resonant island overlap $\chi_e \sim \alpha$, where the island width increases like $\sqrt{\alpha}$. It is also stronger than quadratic power dependence obtained in [6].

Although both the absolute value from the estimate, equation (17), and its dependence on the mode amplitude, $\chi_e \sim \alpha^3$, are in agreement with simulations at $\alpha_0 < 5 \times 10^{-4}$, we observed stronger dependence, $\chi_e \sim \alpha^6$, at higher mode amplitudes, such as shown for $\bar{\psi} = 0.05$. It is possible that higher order nonlinear resonances contribute to the diffusion, but we defer its interpretation to future works. However, we rule out the potential effect of nonlinear high order in α corrections to $E_\parallel$ by carefully examining their contributions numerically using several techniques. The discussion of such effects is presented in appendix A.

Strong amplitude power dependences, $\chi_e \sim \alpha^3$ and $\chi_e \sim \alpha^6$, can introduce intermittently strong e-transport, which can be expected if the GAE amplitude bursts over a short time period. At the same time, measured amplitudes are often obtained from time-averaged data so that the peak GAE amplitude can be higher. The evidence of such behaviour should be reviewed in the experiments. We also note that the collisions have small effects at large mode amplitudes as expected.

Radial dependence of the electron thermal diffusion is determined by the GAE structure assumed in simulations. It is found to be peaked near the mode localization region as shown in figure 9. From these results we can conclude that the marginal agreement between the simulations and $\chi_e > 10\,\mathrm{m^2\,s^{-1}}$ inferred from the experiments can be achieved at the level of mode amplitudes $\alpha > 4 \times 10^{-4}$, which also means that the perturbed magnetic field is $\delta B_r/B >\sim 0.5 \times 10^{-2}$ or $\xi_r/R \sim \alpha(m/k_\parallel r) \sim \alpha/\epsilon \sim 10^{-3}$ and $\delta n/n \simeq \xi_r/R$.

5. Parallel electric field effect on electron transport

Due to small mass electron transport is sensitive to the parallel electric fields. To investigate this effect we use an additional contribution to the electrostatic potential, Ψ, so that $E_\parallel = -\nabla\Psi$, which appears due to thermal ion FLR and is given by equation (7). In this study $E_\parallel$ variation is achieved by changing parameter b_i taken to be the same for all modes for the purpose of illustration. The contribution of Ψ to $E_\perp$ is small, but is a key factor for $E_\parallel$ effects. Depending on the initial radial position, even relatively small $E_\parallel$ can increase thermal electron heat conductivity by as much as an order of magnitude if, for example, b_i changes from zero to $b_i \simeq 10^{-3}$ at $\bar{\psi} = 0.05$ as presented in figure 10.

We observe two characteristic dependences here. Linear dependence, $\chi_e \sim E_\parallel \sim b_i$, is typical and is seen at $\bar{\psi} = 0.06$. On the other hand, from equation (13) it follows that dephasing of electron–GAE interaction is possible due to the parallel electric field. The characteristic time in this case is

$$\tau_{\mathrm{deph}}^{-1} = \frac{k_r k_\theta v_A R_0}{\pi}\alpha b_i.$$

Consequently, we find the heat diffusion coefficient

$$\chi_e = \frac{3}{2}\frac{k_\theta^3 R^3 k_r v_A}{\pi}\alpha^3 b_i. \qquad (18)$$

This expression has the same linear dependence on b_i as seen in the numerical experiment, figure 10. We should note, though, that at certain radii and small values of b_i we find quadratic dependences of the electron heat conductivity, $\chi_e - \chi_{e|E_\parallel=0} \sim E_\parallel^2 \sim b_i^2, b_i < 3 \times 10^{-4}$. One can imagine that at a low parallel electric field the additional contribution to the diffusion comes from the resonant electron displacement (along the lines of [6]), but more detailed study of the phase space maps did not reveal the presence of the resonant structures if multiple modes are included.

Because of the strong effect of the parallel electric field it is important to understand its possible origin. As we saw, the

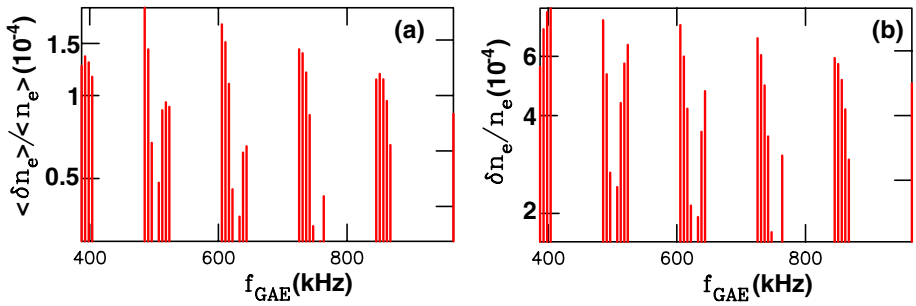

Figure 11. Spectrum of $N = 31$ GAEs used in ORBIT simulations with the amplitude $\alpha_0 = 1.5 \times 10^{-4}$. (*a*) shows a line averaged perturbed density spectrum with the line of sight at $r/a = 0.25$. (*b*) shows the local amplitude of the density perturbation. Plasma rotation with the frequency $f_{\rm rot} = 25$ kHz is taken into account.

perturbative parallel electric field with the ideal MHD limit for $k_\perp$ has negligible effect on the transport. Another effect can be brought up, which is coupling to the KAW. It can potentially introduce strong parallel electric field due to large $k_\perp$.

In the standard GAE theory [2, 15] eigenfrequencies lay below the Alfvénic continuum, where the KAW does not have a propagating wave-like solution. GAEs will have kinetic features with a strong KAW presence if their frequency is above the Alfvén continuum. Such coupling was suggested to exist in stellarators [6]. In tokamaks the theory suggests that the eigenmodes do not always exist in this case. If GAE frequency lays above the continuum maximum (q has a local minimum at some point, $r = r_0$, slightly away from the axis) the criterion for the mode existence was obtained in [19], $Q > 1/4$, where Q is a certain function responsible for the 'effective' potential well. With the expression for Q obtained in high aspect ratio, high-n approximation in [20, 21] this criterion has a form

$$Q \simeq \frac{|n|}{r_0^2 |q_0'' k_\parallel| R_0}\left[\frac{\alpha^2}{2} - \Delta'\alpha + \alpha\varepsilon\frac{q^2-1}{q^2} - \frac{\varepsilon}{2}(\varepsilon + 2\Delta')\right] > \frac{1}{4}, \tag{19}$$

where $\alpha = -R_0 q^2 \beta'$, $\varepsilon = r/R_0$, Δ' is the derivative of the Shafranov shift. In another case when the Alfvén continuum has a minimum (q has a local maximum at $r = r_0$) and GAE frequency lays above it, the criterion for the eigenmode existence can be written in the same form and was obtained in [22]

$$Q > 2. \tag{20}$$

One can see that the second case is more restrictive and requires flatter q profiles. It also follows from both criteria that at sufficiently flat q-profiles (small $r_0^2 q''$) kinetic GAEs can exist.

One particular issue to be resolved is showing that the hybrid kinetic GAE modes are more unstable than the conventional GAEs.

6. Discussion and implications for experiments

Because of the difficulties of measuring the internal mode structures we can compare model GAE spectrum only with the spectrum of the high frequency modes measured by a high-k diagnostic working as an interferometer [23]. The high-k measured high frequency mode spectrum is averaged within 10 ms and has a maximum of the integrated density perturbation on the level of $\langle \delta n_{\rm e}\rangle/\langle n_{\rm e}\rangle \simeq 1.5 \times 10^{-4}$. We show the synthetic diagnostic signal of the used GAE spectrum integrated along the same line as in experiments (see figure 11) with the amplitude $\alpha_0 = 1.5 \times 10^{-4}$, which has to be chosen in such a way that the maximum among all GAE amplitudes fits the measured maximum over the spectrum peaks value $\langle \delta n_{\rm e}\rangle/\langle n_{\rm e}\rangle \simeq 1.5 \times 10^{-4}$. Our plotted spectrum is to be compared with the spectrum shown in figure 4 of [1]. In plotting figure 11 we made use of the following relations:

$$\alpha = \frac{(m-nq)r}{qR_0 m}\frac{\xi_r}{R_0} = \frac{(m-nq)r}{qR_0 m}\frac{\delta n_{\rm e}}{R_0 \nabla n_{\rm e}}. \tag{21}$$

From the latter and figure 11 it follows that approximately we indeed have $\alpha_0 \simeq \langle \delta n_{\rm e}\rangle/\langle n_{\rm e}\rangle$.

One important conclusion to be drawn from figure 11 by comparing (*a*) and (*b*) is that the local value of the density perturbation can be significantly larger than its integral by as much as 5 times. This has to be taken into account when making a comparison with the experiments.

Because of the time averaging used in high-k measurements, GAE peak values within the averaging time interval are larger than the value cited here and in [1] by as much as a factor of 2 or 3. GAE amplitude fluctuation can be seen in the magnetic coil spectrum evolution. We note that the marginal value for the electron heat conductivity inferred from experiments, $\chi_{\rm e} = 10\,{\rm m}^2\,{\rm s}^{-1}$, can be explained by simulations presented in this work given this uncertainty.

In order to make a projection for the electron transport due to multiple GAEs to other fusion experiments one has to predict the number, the structure and the amplitudes of the unstable GAEs. This requires the nonlinear simulations with the capabilities to model the cyclotron resonances in wave–fast particle interactions. These tools are under the development [2, 12]. However, based on this work and previous observations we can draw some qualitative conclusions.

Essential elements of the GAE driven electron transport model presented here for NSTX imply a strong drive on the level $\gamma/\omega = 1$–10% [2] due to strong anisotropy of beam ion velocity distributions. Such anisotropy is also expected for alpha distribution in an ST-like reactor, but less in ITER [24]. GAE instability similar to the ones in NSTX requires a large ratio $v_{\rm f}/v_{\rm A} = 2$–4, which is typical for STs. Weakly damped

multiple instabilities, $N \geqslant 10$, have to be present. Because the drive is proportional to the energy available for the instability, which in turn is proportional to the fast ion beta, β_f, the latter seems to be one of the key parameters responsible for how many GAE instabilities are excited and how virulent they can be. Such conditions mean that relatively high β_f and β_f/β_{pl} are required. Hence, one can conclude that the ST-like fusion reactors are more likely to develop anomalous electron heat transport due to multiple GAE instabilities driven by fusion alpha particles.

7. Summary

We have demonstrated that multiple unstable GAEs with sufficiently strong amplitudes can be responsible for the anomalous electron transport in NSTX. The mechanism for such anomalous transport is stochastic electron radial drift motion in the presence of multiple GAE instabilities. Spacial overlap of multiple instabilities is required for such transport.

Anomalous electron thermal conductivity on the level of $\chi_e = 10\,m^2\,s^{-1}$, which is inferred from TRANSP modelling, is obtained in numerical simulations with $N > 16$ GAEs each having the amplitude of the parallel vector potential $\alpha_0 = 4 \times 10^{-4}$. Within the experimental uncertainties of the mode structure and measured amplitude (factor of 2–3) our simulations produce the required level of electron heat conductivity. Accurate mode identification and structure measurements of high frequency instabilities are needed for better comparison with experiments.

We demonstrated that electron heat conductivity has a strong mode amplitude power dependence ($\chi_e \sim \alpha^3$ and up to $\chi_e \sim \alpha^6$ at high mode amplitudes) and conjecture that it can introduce intermittently strong e-transport. If GAE amplitudes burst over a short time period, GAEs can intermittently induce strong electron diffusion. The evidence of such behaviour should be sought in the experiments. It is interesting that the characteristic magnetic field of the perturbations in our simulations, $\delta B/B \simeq 0.5 \times 10^{-2}$, is the same as used in [7], where the resonant electron–GAE interaction was brought about as a basis for the energy channelling of the heating power from beam ions to GAEs and finally to electrons in the regions outside of the plasma centre. In this mechanism persistent excitation of GAEs is required, implying that almost all the energy from high energy beam ions is transferred to the modes (about half of the injected power comes in low energy ions: at half and one-third fractions of the injection energy). In our mechanism it is possible that GAEs induce electron transport on a short time scale when the perturbation amplitude peaks. In our simulations it is a fraction of a millisecond.

We showed that the perturbed parallel electric field can strongly enhance the radial diffusion. Evidence for $E_\parallel$ presence in experiments have to be sought by resolving ρ_i^{-1} scales. We ruled out the possibility that the nonlinear second order in perturbation correction contributions to the parallel electric field have an effect on the electron thermal diffusion. We would like to note that the interaction between GAEs and the background turbulence can be of interest and has to be studied.

Appendix A. Effect of second order corrections to the parallel electric field on anomalous electron diffusion

As the GAE amplitude increases linear approximation for the derived parallel electric field, equations (5) and (6), may not be accurate beyond some α value. Since the effect of $E_\parallel$ is strong, it is important to investigate such a possibility. We have done two independent checks to address it.

First, $E_\parallel$ is forced to be zero for each particle on its orbit in the equations of motion [18] during the numerical run. Such procedure shows identical results to the baseline cases presented. The problem with it is that the electrostatic potential is not computed using the equation $E_\parallel$ to higher orders and, thus, changes electron Hamiltonian.

The second method is to directly compute the second order contributions. It allows for self-consistent evaluation of the electrostatic potential to satisfy the ideal MHD requirement $E_\parallel = 0$ to that second order in α. This method after implementation in the ORBIT code produces again almost identical results to the ones presented in this paper. We derive the expression for ϕ hereafter, where we employ the same notations as in [18].

Let us expand the electrostatic potential

$$\phi = \phi_0 + \phi_1, \tag{A1}$$

where ϕ_0 is the linear in $\alpha \ll 1$ approximation and ϕ_1 is the second order correction. The linear part of the electrostatic potential satisfies

$$\nabla_\parallel \phi_0 = \frac{i\omega}{c}\alpha B_0, \tag{A2}$$

which results in equation (6). The second order correction can be found from the following equation

$$\nabla_\parallel \phi_1 = -\frac{\delta \boldsymbol{B}}{B_0}\nabla\phi_0 + \frac{i\omega}{c}\alpha\delta B_\parallel, \tag{A3}$$

where higher order terms were ignored.

We also have for the parallel to the magnetic field operator

$$\nabla_\parallel = \frac{1}{B_0 J}(\partial_\theta + q\partial_\varphi),$$

where J is the Jacobian satisfying the case of the Boozer equilibrium $B^2 J = I + gq$ and $g = B_{0\varphi}R$. Using equation (A2) we find that only $\delta \boldsymbol{B}_\perp$ contributes and

$$\nabla_\parallel \phi_1 = -\frac{\nabla_\perp \phi_0}{B_0}[\nabla\alpha \times \boldsymbol{B}_0 + \alpha\nabla \times \boldsymbol{B}_0]. \tag{A4}$$

After some algebra and assuming $\alpha = \sum_j \alpha_j \sin P_j$, where P_j is the phase, we find

$$\begin{aligned} J B_0 \nabla\phi_1 = {} & \sum_{j',j}\left(\frac{I+gq}{n'q-m'}\right)'_\psi \omega_{j'}\alpha_{j'}\sin P_{j'} \\ & \times\left[\frac{\nabla\psi^2}{X^2}\alpha_j n J\cos P_j + mg\alpha_j\cos P_j\right] \\ & - \omega\alpha_{j'}\sin P_{j'}\alpha_j\cos P_j[g' B_0^2 J + J g p'] \\ & - \alpha_{j'}\sin P_{j'}\phi_{0j} n\cos P_j J\nabla\frac{\nabla\psi}{X^2} \\ & - \alpha_{j'}\sin P_{j'}\phi_{0j} m\cos P_j g', \end{aligned} \tag{A5}$$

where primes in the mode numbers and frequency mean that they are related to j' sum.

References

[1] Stutman D., Delgado-Aparicio L., Gorelenkov N., Finkenthal M., Fredrickson E., Kaye S., Mazzucato E. and Tritz K. 2009 *Phys. Rev. Lett.* **102** 115002

[2] Gorelenkov N.N., Fredrickson E.D., Belova E., Cheng C.Z., Gates D., Kaye S. and White R.B. 2003 *Nucl. Fusion* **43** 228

[3] Ono M. *et al* 2000 *Nucl. Fusion* **40** 557

[4] Gorelenkov N.N., Boozer A., Stutman D., Fredrickson E., Tritz K. and White R. 2009 *Bull. Am. Phys. Soc.* **54** 238 (abstract PP8.61, http://meetings.aps.org/link/BAPS.2009.DPP.PP8.61)

[5] White R.B. and Chance M.S. 1984 *Phys. Fluids* **27** 2455

[6] Kolesnichenko Ya.I., Yakovenko Yu.V. and Lutsenko V. 2010 *Phys. Rev. Lett.* **104** 075001

[7] Kolesnichenko Y.I., Yakovenko Y.V. and Lutsenko V. 2010 *Phys. Rev. Lett.* **94** 075001

[8] Stutman D., Tritz K., Delgado-Aparicio L., Finkenthal M., Kaye S., Bell M., Bell R., Kugel H., LeBlanc B. and Yuh H. 2007 *34th European Physical Society Conf. on Plasma Physics, Warsaw, Poland, 2–6 July 2007* P2.061

[9] Gates D., Gorelenkov N.N. and White R.B. 2001 *Phys. Rev. Lett.* **87** 205003

[10] Tritz K. *et al* 2008 *Phys. Plasmas* **15** 056119

[11] Fredrickson E.D., Gorelenkov N.N. and Menard J. 2004 *Phys. Plasmas* **11** 3653

[12] Belova E.V., Gorelenkov N.N. and Cheng C.Z. 2003 *Phys. Plasmas* **10** 3240

[13] Gorelenkov N., Fredrickson E., Heidbrink W., Crocker N., Kubota S. and Peebles W. 2006 *Nucl. Fusion* **46** S933

[14] Smith H.M. and Verwichte E. 2009 *Plasma Phys. Control. Fusion* **51** 075001

[15] Mahajan S.M. and Ross D.W. 1983 *Phys. Fluids* **26** 2195

[16] Gorelenkov N.N., Belova E., Berk H.L., Cheng C.Z., Fredrickson E.D., Heidbrink W.W., Kaye S. and Kramer G.J. 2004 *Phys. Plasmas* **11** 2586

[17] Cheng C.Z. and Gorelenkov N.N. 2004 *Phys. Plasmas* **11** 4784

[18] White R.B. 2001 *The Theory of Toroidally Confined Plasmas* 2nd edn (London: Imperial College Press)

[19] Berk H.L., Borba D.N., Breizman B.N., Pinches S.D. and Sharapov S.E. 2001 *Phys. Rev. Lett.* **87** 185002

[20] Fu G.Y. and Berk H.L. 2006 *Phys. Plasmas* **13** 052502

[21] Gorelenkov N., Kramer G. and Nazikian R. 2006 *Plasma Phys. Control. Fusion* **48** 1255

[22] Gorelenkov N.N. 2008 *Phys. Plasmas* **15** 110701

[23] Mazzucato E. 2006 *Plasma Phys. Control. Fusion* **48** 1749

[24] Gorelenkov N.N. 1992 *Fiz. Plasmy* [*Sov. J. Plasma Phys.*] **18** 289 **18** 555